Lasers in Surgery and Medicine 28:103–112 (2001)

Cryogen Spray Cooling: Effects of Droplet Size and Spray Density on Heat Removal

Brian M. Pikkula, BS, Jorge H. Torres, MD. PhD, James W. Tunnell, BS, and Bahman Anvari, PhD*
Department of Bioengineering, Rice University, Houston, Texas 77251

Background and Objective: Cryogen spray cooling (CSC) is an effective method to reduce or eliminate non-specific injury to the epidermis during laser treatment of various dermatological disorders. In previous CSC investigations, fuel injectors have been used to deliver the cryogen onto the skin surface. The objective of this study was to examine cryogen atomization and heat removal characteristics of various cryogen delivery devices.
Study Design/Materials and Methods: Various cryogen delivery device types including fuel injectors, atomizers, and a device currently used in clinical settings were investigated. Cryogen mass was measured at the delivery device output orifice. Cryogen droplet size profiling for various cryogen delivery devices was estimated by optically imaging the droplets in flight. Heat removal for various cryogen delivery devices was estimated over a range of spraying distances by temperature measurements in an skin phantom used in conjunction with an inverse heat conduction model.
Results: A substantial range of mass outputs were measured for the cryogen delivery devices while heat removal varied by less than a factor of two. Droplet profiling demonstrated differences in droplet size and spray density.
Conclusions: Results of this study show that variation in heat removal by different cryogen delivery devices is modest despite the relatively large difference in cryogen mass output and droplet size. A non-linear relationship between heat removal by various devices and droplet size and spray density was observed. Lasers Surg. Med. 28:103–112, 2001. © 2001 Wiley-Liss, Inc.

Key words: dermatology; heat removal; hypervascular lesions; non-ablative resurfacing; port-wine stain; refrigerant atomization; selective thermal injury

INTRODUCTION

The growth of laser technology and the relative non-invasiveness of dermatological laser surgery has lead to a dramatic increase of cutaneous laser procedures over the past two decades. Laser irradiation is currently used for removal of hair [1,2], facial rhytides [3], tattoos [4], and hypervascular lesions such as port-wine stains [5]. The unwanted dermal structures are targeted by prescribing a particular wavelength which is preferentially absorbed by the targeted chromophore (e.g., melanin, collagen, tattoo ink, or hemoglobin), and specifying an appropriately short laser pulse to limit thermal diffusion away from the targeted chromophore into the surrounding tissue [6]. Targeted chromophores subsequently undergo photothermolysis, in which the energy deposited to the desired site results in thermal destruction of these structures [6]. Despite the selection of an appropriate wavelength for the targeted chromophore, light absorption by the overlying epidermal melanin which takes place over a broad spectral bandwidth [7] can result in non-specific heating of the epidermis.

Protecting the epidermis from non-specific heating can be accomplished by precooling the skin prior to laser irradiation with methods such as sapphire contact and cryogen spray cooling [3,8–11]. Immediately following pulsed laser irradiation, the precooled epidermis is heated to a temperature below the threshold for thermal injury. With cryogen spray cooling (CSC), a short (on the order of tens of milliseconds) cryogen spurt is sprayed onto the skin surface just prior to laser irradiation. CSC has been shown to protect the epidermis from non-specific thermal injury during cutaneous laser applications [10,12–14].

In previous CSC studies, fuel injectors have been used as the cryogen delivery device [11,15–18]. The objective of this study was to examine cryogen atomization by various delivery devices, and to evaluate their heat removal effectiveness (i.e., substrate temperature reductions and total heat removal).

MATERIALS AND METHODS

Cryogen Delivery Devices

Four types of delivery devices were utilized in this study (Table 1). They consisted of:

(1) a fuel injector with a 1.3-mm diameter orifice which has been used in our previous studies [15,16,18];
(2) a second fuel injector with a 1-mm diameter orifice which originally produced a hollow cone spray pattern (but was modified with attachment nozzles of either a 1- or 1.5-mm orifice diameter in order to ensure a uniform spray pattern on the substrate surface);

Contract grant sponsor: The Whitaker Foundation and National Science Foundation; Contract grant number: BES-9896101.
*Correspondence to: Bahman Anvari, Department of Bioengineering, MS 142, Rice University, P.O. Box 1892, Houston, TX 77251. E-mail: anvari@rice.edu
Accepted 27 November 2000

TABLE 1. Designations for Cryogen Delivery Devices used in this Study

Fuel injector #1. Orifice diameter: 1.3 mm. No attachment nozzle	A
Fuel injector #2. Orifice diameter: 1.0 mm. Attachment nozzle orifice diameter: 1.0 mm	B
Fuel injector #2. Orifice diameter: 1.0 mm. Attachment nozzle orifice diameter: 1.5 mm	C
Commercial atomizer. Orifice diameter: 1.0 mm. No attachment nozzle	D
Commercial atomizer Orifice diameter: 1.5 mm No attachment nozzle	E
Cryogen delivery device incorporated with the ScleroPlus™ laser. Orifice diameter: 0.75 mm. No attachment nozzle	F

(3) commercially available atomizers (SU11-2050 and SU22B-40100, Spraying Systems Co., Wheaton, IL) with 1- and 1.5-mm orifice diameters, respectively; and
(4) a cryogen delivery device with an orifice diameter of 0.75 mm incorporated in the ScleroPlus™ laser (Candela Corp., Wayland, MA) which is used clinically to treat hypervascular cutaneous malformations such as port-wine stains.

Orifice diameters for the second fuel injector and commercial atomizers were chosen to cover a relatively wide range, between 0.75 and 1.5 mm. For the remainder of the manuscript, cryogen delivery devices will be referred to as described in Table 1.

Cryogen R-134a (1,1,1,2 tetrafluoroethane) (National Refrigerants, Inc., Rosenhayn, NJ) a non-toxic, environmentally compatible, Freon substitute [19,20] (boiling point $\approx -26^{\circ}C$ at 1 atm), utilized for epidermal protection and pain reduction during cutaneous laser procedures was used in this study. Excluding the ScleroPlus™, which has its own hardware and timing software, cryogen spurt duration was controlled by a programmable digital delay generator (DG535, Stanford Research Systems, Sunnyvale, CA) in conjunction with a relay circuit. Cryogen spurts with durations (τ) of 100 and 200 ms from various distances (10–130 mm) were applied onto a test substrate positioned normal to the cryogen delivery device, and the resulting internal temperature profiles were recorded (Fig. 1a).

Cryogen Mass Output Measurements

Cryogen mass output at the tip of each cryogen delivery device was measured by collecting the sprayed volume into a large, evacuated balloon and measuring the increase in mass of the balloon. These experiments were repeated four times for each cryogen delivery device. Alternatively, the sprayed volume was estimated by measuring the displaced volume of water within a graduated cylinder in which the

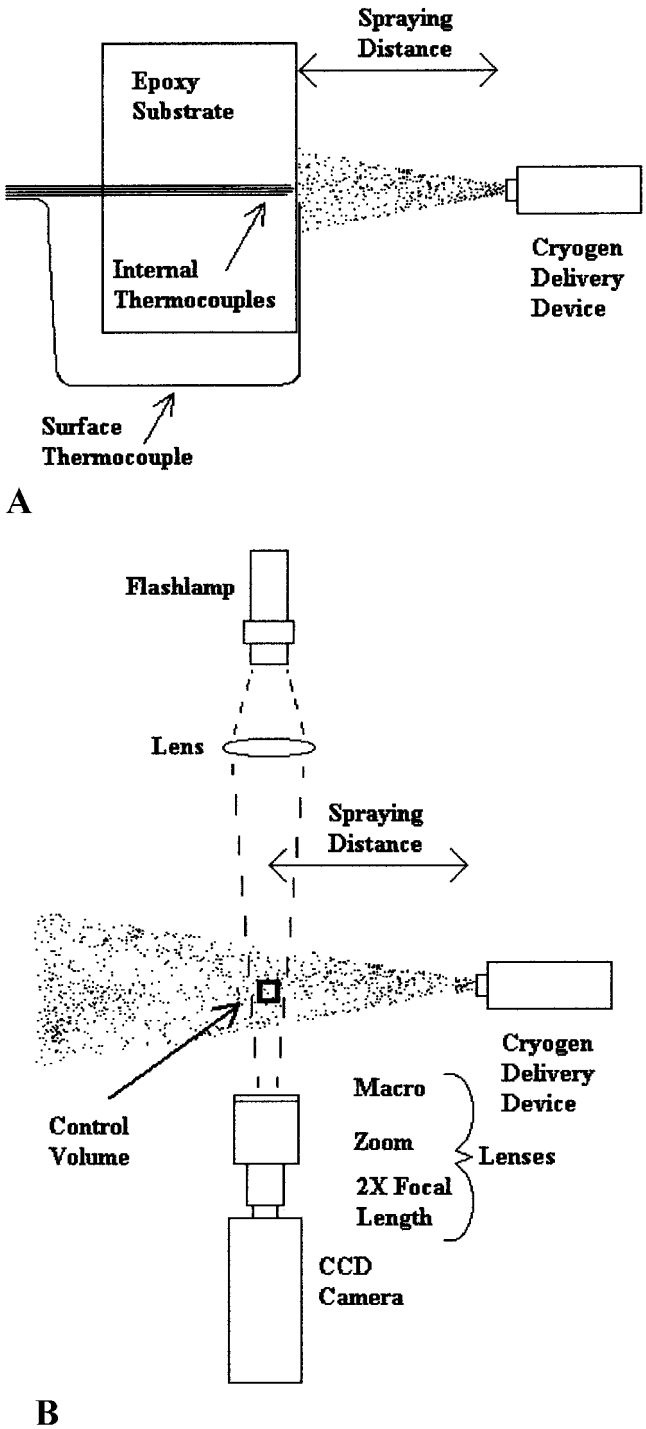

Fig. 1. Schematic of the setup used for: (**A**) temperature measurements in vitro; and (**B**) cryogen droplet imaging and size profiling.

balloon was immersed. Subsequently, the cryogen mass output was estimated using the density of the cryogen gas (3.8 kg/m^3 at 1 atm and room temperature) and the displaced volume measurements. The volume of the balloon was greater than twice the volume of the cryogen gas (evaporated liquid) to ensure that no pressure was exerted on the cryogen gas to alter its density. The two techniques gave mass output measurements that were within 15–20% of each other.

Cryogen Droplet Size Profiling

Cryogen droplet size distributions from the various delivery devices were quantified by an optical imaging system. A CCD camera (MegaPlus ES310, Eastman Kodak, San Diego, CA) and a zoom-macro lens (Zoom 7000, Navitar, Japan) with a 2X focal length extender (EX2C, Computar CBC AMERICA Corp., Commack, NY) for further magnification were used to image the cryogen droplets in flight. The respective depth of field, width, and height of the imaged volume were 1.3, 1.5 and 1.5 mm, giving a control volume of approximately 2.9 mm^3. A 20-ns duration flashlamp (NANOLITE, High-Speed Photo-Systeme, Germany) with emitted light focused along the optical axis of the camera (Fig. 1b) was used as the illumination source. The cryogen was sprayed perpendicular to the optical axis of the camera and flashlamp. A frame grabber was used to capture the images and save them to a desktop computer. Resolution of the imaging system (inter-pixel distance) was 3.16 μm/pixel which was determined by dividing the image height (1.5 mm) by the number of pixel rows (480). We were able to resolve a droplet that covered a 3×3 pixel area which resulted in a minimum resolvable droplet diameter of 9.5 μm. Thresholding, counting, and particle sizing was accomplished by NIH Scion Image (http://www.scioncorp.com) analysis software, except analysis of the droplets sprayed by the delivery device F, which due to the high droplet density, was done manually.

Droplet size was characterized in two ways. First, using the simple arithmetic mean diameter obtained by direct particle sizing from the image. Second, utilizing the Sauter mean diameter (SMD), which is commonly used to quantify droplet size during spraying processes [21,22]. The SMD is the diameter of a droplet whose volume-to-surface ratio is equivalent to the ratio of the sum of the volume to the sum of the surface area of all droplets in the imaged droplet set:

$$\mathrm{SMD} = \frac{\sum_{i=1}^{N} D_i^3 n_i}{\sum_{i=1}^{N} D_i^2 n_i} \tag{1}$$

In the above equation, D is the median droplet diameter of the given bin, n the number of droplets in that bin, i the bin number, and N the total number of bins. Droplets were assigned to bins which represent droplet diameters 1–4, 5–8, 9–12, ... 197–200, and 200 + μm.

As stated above, the optical imaging system was unable to resolve droplets that have a diameter less than 9.5 μm; therefore, bins 1–4 and 5–8 μm were extrapolated by the Rosin–Rammler expression for drop size distribution [21]. The Rosin–Rammler expression allows for small droplet diameters to be extrapolated, generally where particle sizing is least accurate (i.e., for small droplets). Extrapolation was achieved by plotting $\ln(1 - \mathrm{P})^{-1}$ as a function of droplet diameter, D, where P is the fraction of the total volume contained by drops of diameter less than D. Values in Table 2 reflect information including the extrapolated bins.

Temperature Measurements

Although it would be desirable to determine the heat removed by various cryogen delivery devices from skin, it is not a trivial task to make the appropriate temperature measurements in vivo or within ex vivo samples. A skin phantom was constructed [15,18] from epoxy resin (EP30, Master Bond Inc., Hackensack NJ) with thermal diffusivity of 0.7×10^{-7} m^2/s, within 36% of that of skin, 1.1×10^{-7} m^2/s [23]. An epoxy resin phantom has also been used by other investigators [17]. Good agreement between computed temperature profiles, and those measured in the epoxy model have been obtained [18], demonstrating the usefulness of the epoxy substrate as an experimental model to investigate the effects of various

TABLE 2. Comparison of Q (at Spurt Termination), Mass Output, Average Droplet Diameter, SMD, Spray Density, ΔT_{0^-}, and $D_{Q_{max}}$ for All Cryogen Delivery Devices at Each $D_{Q_{max}}$ Arranged in Order of Decreasing Q for a 200-ms Spurt

Cryogen delivery device	Q (kJ/m^2)	Mass output (mg)	Average droplet size (μm)	SMD (μm)	Spray density (droplets/mm^3)	ΔT_{0^-} (°C)	$D_{Q_{max}}$ (mm)
C	11.83 (±0.15)	519.6 (±3.2)	25.9 ± 2.1	65.9	226 ± 17	75	100
E	11.41 (±0.08)	188.1 (±3.6)	24.6 ± 2.0	62.4	173 ± 20	72	40
B	11.31 (±0.07)	476.1 (±4.0)	23.9 ± 2.4	62.3	205 ± 22	71	60
D	11.11 (±0.15)	70.0 (±5.5)	30.4 ± 2.8	85.6	159 ± 16	76	40
F	10.41 (±0.08)	242[a]	16.2 ± 1.8	38.3	286 ± 28	66	40
A	10.36 (±0.06)	492.8 (±10.8)	34.0 ± 3.7	116.1	136 ± 18	66	90

[a](Candela Laser Corp., personal communication).

CSC parameters in a non-degrading medium which can be repeatedly used.

Type K thermocouples (Chromega® Alomega®, Omega Engineering, Inc., Stamford, CT), with a bead diameter of 30 μm and lead diameters of ≈13 μm were imbedded at known depths (20, 90, 200, and 400 ± 5 μm). Additionally, a surface thermocouple, type E, 300 μm bead, (Chromega® Constantan, Omega Engineering, Inc., Stamford, CT) was used to record the cryogen film temperature (T_{film}) (Fig. 1a). All thermocouples were connected to an external 14-bit A/D converter (instruNet Direct Sensor to-Data Acquisition system, Omega Engineering Inc., Stamford, CT).

Temperature reductions in response to CSC were the difference between the initial substrate temperature (T_{i}) and the measured internal temperature ($T(x)$) (where x is the depth within the epoxy resin substrate). The temperature reduction just above the substrate surface (ΔT_0-) measured by the surface thermocouple, was defined as $T_{\text{a}} - T_{\text{film}}$ where T_{a} was the ambient room temperature.

Heat Removal Estimation

Inasmuch as thermal boundary conditions such as a time-varying heat flux ($q(t)$) are difficult to measure directly, indirect techniques using internal temperature measurements are often used [24]. With these techniques, an inverse heat conduction problem (IHCP) is solved to estimate the boundary condition from internal temperature measurements. We used the sequential function specification (SFS) method [25] to solve the IHCP from temperature measurement at a known depth within the epoxy-resin substrate at discrete times. The SFS technique is capable of resolving fast transients in surface heat flux and has been used in similar types of experiments to estimate $q(t)$ during metal quenching and metal–metal contact experiments [26–28].

Details of the SFS method are described in another manuscript from our group [29], where the accuracy of the technique is verified by comparison with known solutions. Here we only seek to give a brief overview of the method. The SFS method estimates the surface heat flux as a piecewise function of time, sequentially solving for $q(t)$ at each time point. In doing so, the method uses "future" temperature data to estimate the surface heat flux at the current time point. The method becomes more stable as the number of future times (R) is increased.

The SFS technique minimizes the following least squares expression over R future time steps

$$\Delta = \sum_{r=1}^{R} (U(x_i, t_r) - T(x_i, q(t_r)))^2 \rightarrow \min \qquad (2)$$

where $U(x_i, t_m)$ is the measured temperature, and $T(x_i, q(t_m))$ is the estimated temperature at time t_{m} and depth x_{i}. Using Duhamel's theorem and a sensitivity coefficient $Z(x_i, t_m)$ [25], the temperature distribution is represented by

$$T(x_i, q(t_m)) = T(x_i, q(t_{m-1})) + Z(x_i, t_m)(q(t_m) - q(t_{m-1})) \qquad (3)$$

The sensitivity coefficient represents the temperature distribution due to a unit step in surface heat flux. Assuming that the heat flux history is known up to time point t_{m-1}, the only unknown in equation (3) is the heat flux at time t_m. Substituting equation (3) into equation (2), we solve a least squares equation to get the unknown heat flux $q(t_m)$. The minimization of the least squares norm over R future times guarantees the existence of a solution to this inverse problem [30]. The sensitivity of the IHCP is described fully in [29], but for the purposes of this manuscript, a ± 10% uncertainty in thermal conductivity results in a maximum ± 5% deviation in the instantaneous surface heat flux.

The total heat removal per unit area, Q (J/m^2), the time-integral of $q(t)$, was determined from the solution of the IHCP for the various cryogen delivery devices. The IHCP estimates Q through the surface area directly above the 20-μm deep thermocouple for which heat removal is assumed to be uniform over a diameter equivalent for a laser spot size of 7 mm. Calculated as a function of spraying distance (average of three spurts for each device and distance), Q attains a maximum ($Q_{\max}$) at a distinct spraying distance ($D_{Q_{\max}}$) which can be seen in Figure 5. Although heat is removed following the spurt termination due to a cryogen film residing on the substrate surface, all reported values of heat removal in this study will be $Q_{\max}$ for each cryogen delivery device, at the respective $D_{Q_{\max}}$, immediately upon termination of the spurt. Plots with error bars and numerical values in the text and tables are averages (± SD).

RESULTS

Cryogen Mass Output Measurements

The mass output of a 200-ms spurt at the tip of each of the cryogen delivery devices is shown in Table 2. Due to the design of cryogen delivery device F, we were unable to determine the mass output by our method. The volumetric flow rate of cryogen delivery device F is approximately 1 μL/ms (Candela Laser Corp., personal communication) which is equivalent to a mass flow rate of 1.21 mg/ms. Therefore, the mass output for a 200-ms spurt for cryogen delivery device F was approximately 242 mg.

Despite the great differences among the mass output of the cryogen delivery devices tested, the total heat removed for the duration of the spurt per area is comparable. For example, the mass outputs of cryogen delivery device C and cryogen delivery device D were 519.6 (± 3.2) and 70.0 (± 5.5) mg, respectively, while the total heat removed was relatively similar at 11.83 (± 0.15) and 11.11 (± 0.15) kJ/m^2 (Table 2). This result suggests that certain cryogen delivery devices may be inefficient (i.e., a low ratio of heat removed/mass output) in terms of heat extracted per mass output as compared with other devices. The effect of greater mass output present on the substrate surface, however, results in increased heat removal *after* the spurt termination due to the longer residence time.

Although the total mass output varied by more than a factor of seven, the mass output per unit area on the substrate surface was much more comparable. At a spraying

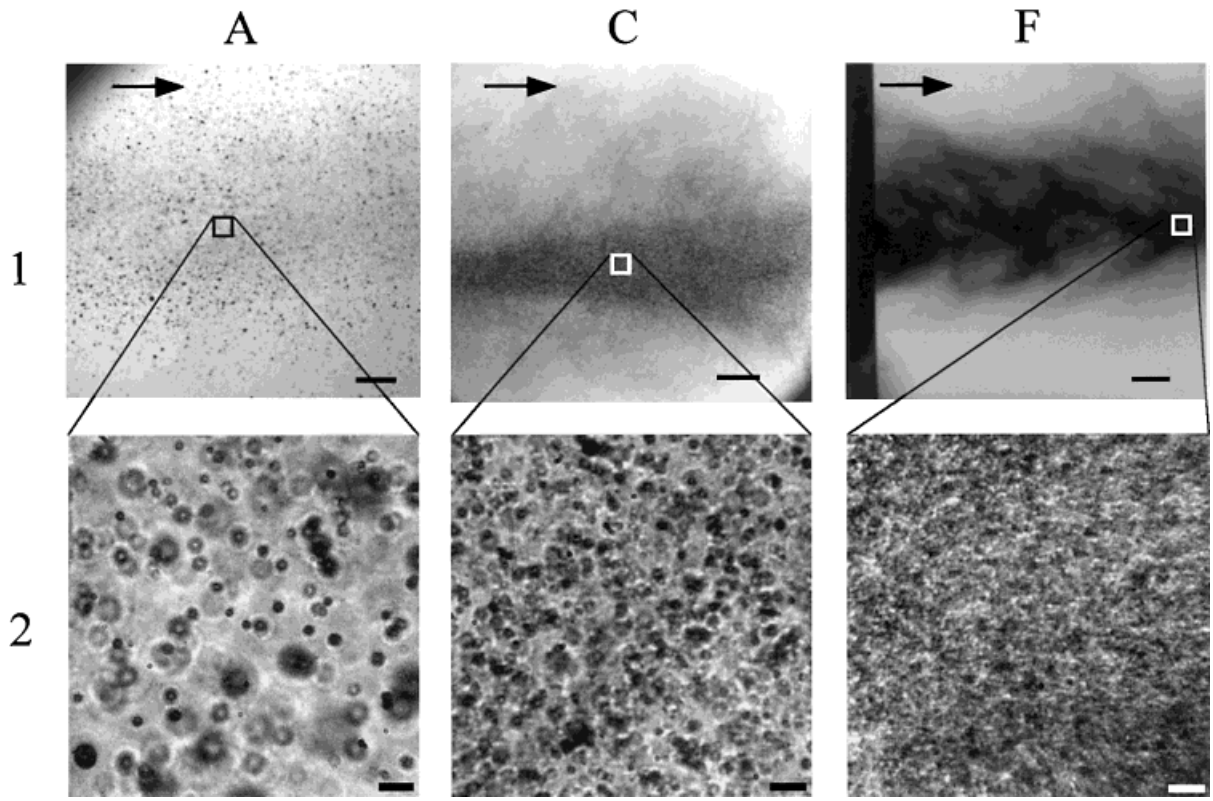

Fig. 2. Images of droplets at $D_{Q_{max}}$. Columns A, C and F correspond to images of droplets sprayed by cryogen delivery devices A, C and F, respectively. Images in row 1 are the gross spray images with the bar equal to 2 mm. Images in row 2 are those used to analyze droplet size and spray density (bar represents 100 μm). Arrow is direction of spray. *Note*: Images 2 are not enlargements of images 1.

distance of $D_{Q_{max}}$, the respective sprayed areas, measured by a ruler and confirmed by captured images, for devices C and D were 30 and 8 mm, respectively; resulting in mass outputs per unit area of 0.74 and 1.4 mg/mm^2. Despite a factor of 7 difference in total mass output and assuming evaporation in flight proportionate to mass output, the mass per area (i.e., relative height of the film) varies by less than a factor of 2.

Cryogen Droplet Size Profiling

Figure 2 is a two-dimensional representation of a three-dimensional volume; therefore, an error in the imaging method presented above is the obstruction of one droplet by another. To model the probability of a droplet being hidden by another, we present the following analysis. Assuming uniform spatial distribution and 30-μm diameter drops, the 1.5×1.5 mm image was divided into 50 rows and 50 columns, resulting in 2,500 compartments for an average of 600 droplets (based on histograms) to occupy. A random number generator then assigned each of the 600 drops to a compartment. If a compartment contained more than one droplet, the compartment was identified as such. The likelihood of one and two hidden droplets was 9.5 and $<1\%$, respectively (determined by more than one droplet in a compartment). Therefore, the number of droplets hidden is 67.5 (± 8) droplets. Of the 600 droplets imaged by the CCD camera, 68 are considered unaccounted for, resulting in a total of 668 droplets with a difference between the calculated and imaged set of 11%. All delivery devices will have a similar shift to a greater number of actual droplets (spray density), and since a random distribution of droplets is assumed, there should be no change in the calculated droplet diameter. The reported values in Table 2 do not account for any hidden droplets.

Due to the visual similarities of droplet images produced by cryogen delivery devices B–E, we only present the images for devices A, C, and F (Fig. 2). The droplets in the control volume appear as dark areas in the image, due to scattering of light by the droplets. Shown in Table 2, arranged in order of decreasing Q, is the average droplet size, SMD, and spray density.

Figure 3 are histograms of droplet size distribution for the various cryogen delivery devices at their respective $D_{Q_{max}}$. The resulting histograms of devices B-E are similar; therefore, only histograms from devices A, C, and F are presented. The low spray density and large droplet size of cryogen delivery device A can be easily observed in Figure 2 image A and Figure 3, histogram labeled A. In contrast to cryogen delivery device A is the device F, which produces

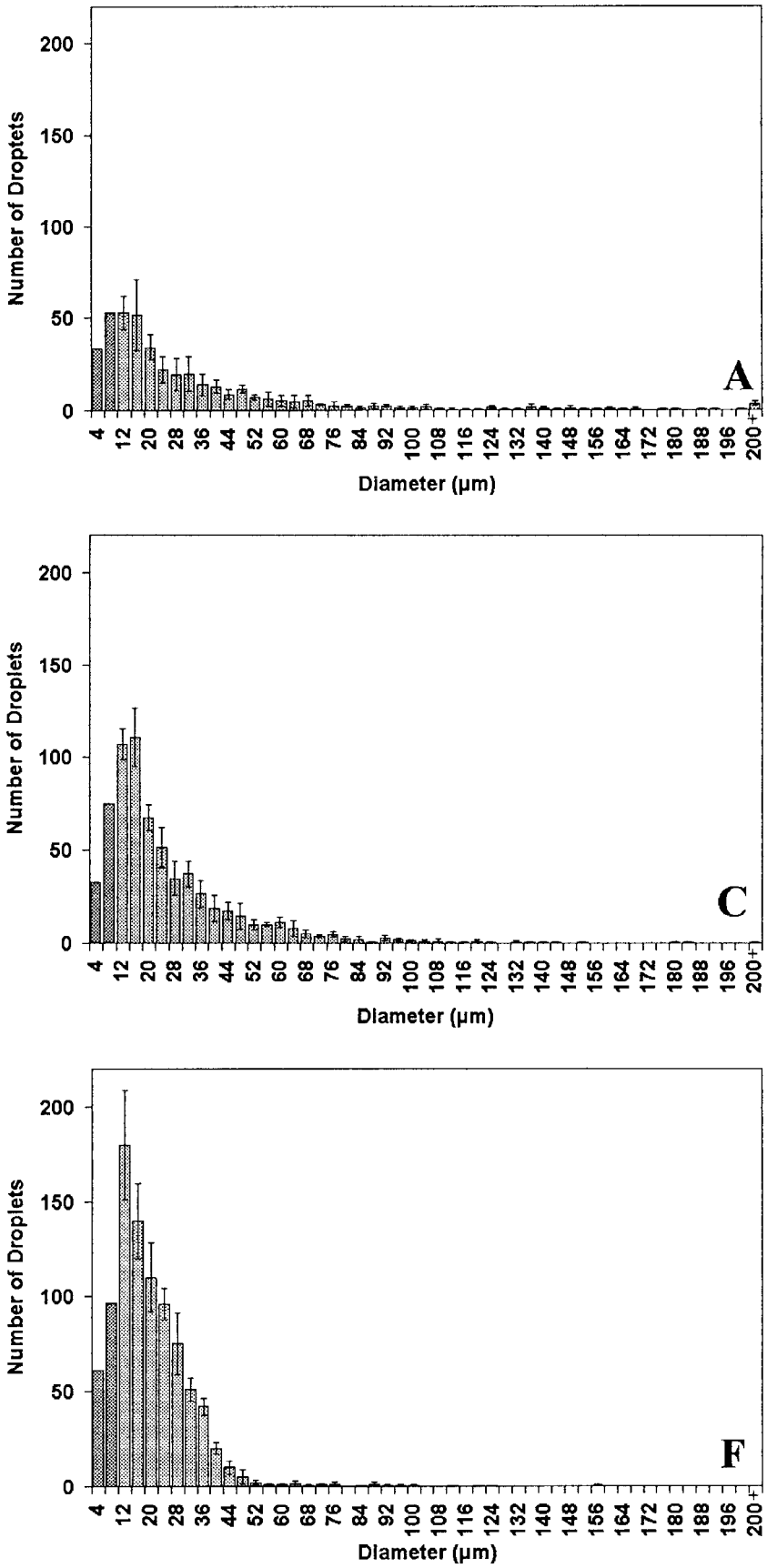

Fig. 3. Histograms of droplet size distribution for delivery device A, C, and F at the spraying distance ($D_{Q_{max}}$) where maximal heat removal was achieved. Each bin size is 4 μm with the numerical designation on the abscissa indicating the upper bound of the bin. Therefore, the bins 1–4, 5–8, 9–12, and 13–16 μm, etc., are designated 4, 8, 12, and 16, respectively.

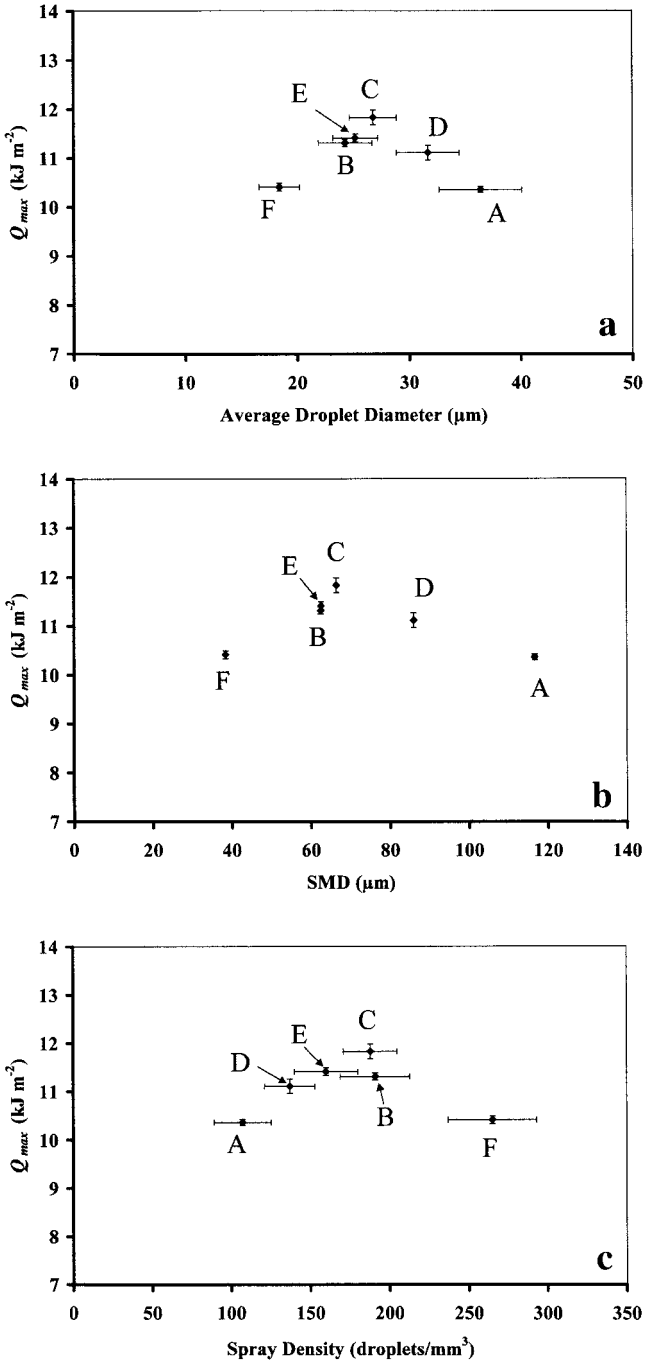

Fig. 4. Maximal heat removal ($Q_{\max}$) achieved at spraying distance $D_{Q_{\max}}$ immediately upon termination of a 200-ms spurt as a function of (**a**) average diameter, (**b**) SMD, and (**c**) spray density for the six cryogen delivery devices.

high spray density and small droplet diameter (Fig. 2, image F; Fig. 3, histogram labeled F). A parabolic trend appears in relating Q to the average diameter of the droplets, SMD, and spray density (Fig. 4). Note that the order of cryogen delivery devices in Figure 4c changes when compared to those in Figure 4a and 4b. It appears that a device producing low spray density and relatively large droplets (device A) removes the same amount of heat as a device which produces high spray density but with small droplets (device F). With the median droplet size and spray density, cryogen delivery device C produces the greatest $Q_{\max}$ of the devices tested (Fig. 4a–c) suggesting that a combination of spray density and droplet size may partially account for maximum heat removal. Despite these trends, as described further in the Discussion section, these may not be the only parameters involved in optimizing heat removal.

Temperature Measurements and Heat Removal Estimations

Increasing the spraying distance resulted in elevated values of ΔT_{0^-} up to a critical distance, beyond which ΔT_{0^-} decreased (Fig. 5). For devices D and F this pattern would have been expected if greater spraying distances had been used for experimentation. Similarly, Q reached a local maximum ($Q_{\max}$) and then decreased beyond a certain spraying distance ($D_{Q_{\max}}$) (Fig. 5). For cryogen delivery device F (limited to a 100-ms spurt duration), a 100-ms spurt removed 6.15 ± 0.05 kJ/m^2, and a 200-ms spurt, predicted by an experimental relationship (discussed below), is expected to remove 10.41 ± 0.08 kJ/m^2.

Due to the similarities in the thermal properties of skin and epoxy phantom, a physiological relevant depth of 90 μm was chosen for examining temperature reductions, which corresponds to a realistic depth of the epidermal basal layer in human skin. The temperature reduction $\Delta T_{90\,\mu m} = T_i - T(\tau = 200\text{ms})|_{x=90\,\mu m}$, as a function of spraying distance, is proportional to Q for a 200-ms spurt for all cryogen delivery devices examined (Fig. 5). The values of $Q_{\max}$ for each device are strongly correlated ($r > +0.99$) to the temperature reductions at $x = 90$ μm ($\Delta T_{90\mu m}$) for *different* cryogen delivery devices delivering equal spurt durations (Fig. 6).

Heat removal, $Q(t)$, (achieved at spraying distance $D_{Q_{\max}}$) in response to a 200-ms spurt for the cryogen delivery devices A–E is shown in Figure 7a. Three different intervals (S, R, and I) corresponding to spraying time, cryogen residence time, and the presence of ice on the substrate surface, respectively, can be seen (Fig. 7b). Different rates of heat extraction in the S interval provide an explanation to the differences of Q in Table 2. Fig. 7b is a plot of Q (t) in response to 100 and 200-ms spurts from cryogen delivery device C. As seen in Figure 7b, a 200-ms spurt can remove approximately 70% more heat than a 100-ms spurt. In contrast, only 21% more heat is removed after 100 ms following termination of a 100-ms spurt. Consistent with results of theoretical modeling in Ref. [31], the highest rate of heat extraction occurs during the spraying time (S). The R interval for the 200-ms spurt is approximately 32% longer than the same interval for the 100-ms spurt due to the greater mass output of the longer spurt.

During the film residence time (interval R), a nearly constant slope of approximately 20 kW/m^2 is an indication that the residing cryogen film on the substrate surface removes heat equally well despite its initial atomization

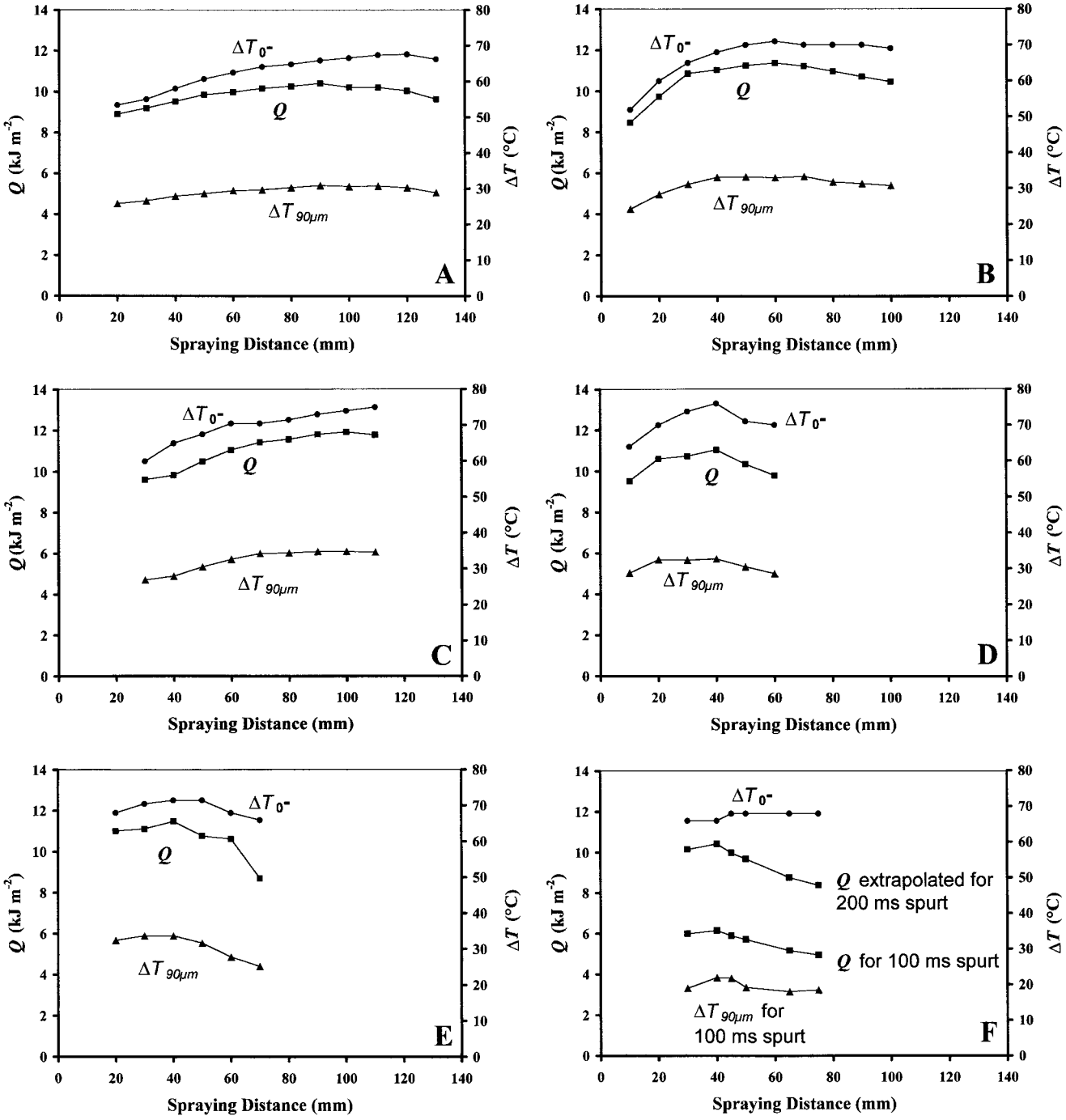

Fig. 5. Averaged values for temperature reductions just above the substrate surface, (ΔT_{0^-}) (●), temperature reductions at 90 μm, $\Delta T_{90\,\mu m}$ (▲), and total heat removed Q (■), for devices **A–F** as a function of spraying distance at the end of a 200-ms spurt.

or deposition. From the recorded temperature profiles and video images of the sprayed substrate [32], ice was determined to form at the points indicated by the arrows (Fig. 7b), and remained during the entire I interval. This interval occurs after the cryogen film evaporation, and the presence of ice results in a relatively low and nearly constant rate of heat removal.

DISCUSSION

Melanin offers two obstacles to cutaneous laser treatment: (1) it absorbs the incident laser energy; hence, it decreases the therapeutic light dosage reaching the intended dermal targets; and (2) the light energy absorbed by melanin can cause non-specific thermal injury. Inas-

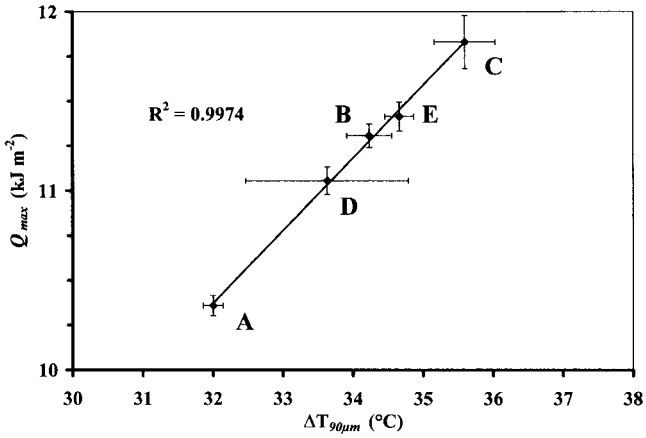

Fig. 6. Correlation between $Q_{\max}$ from a 200-ms spurt and temperature reduction at 90 μm below the epoxy resin substrate surface ($\Delta T_{90\,\mu m}$) for cryogen delivery devices A–E.

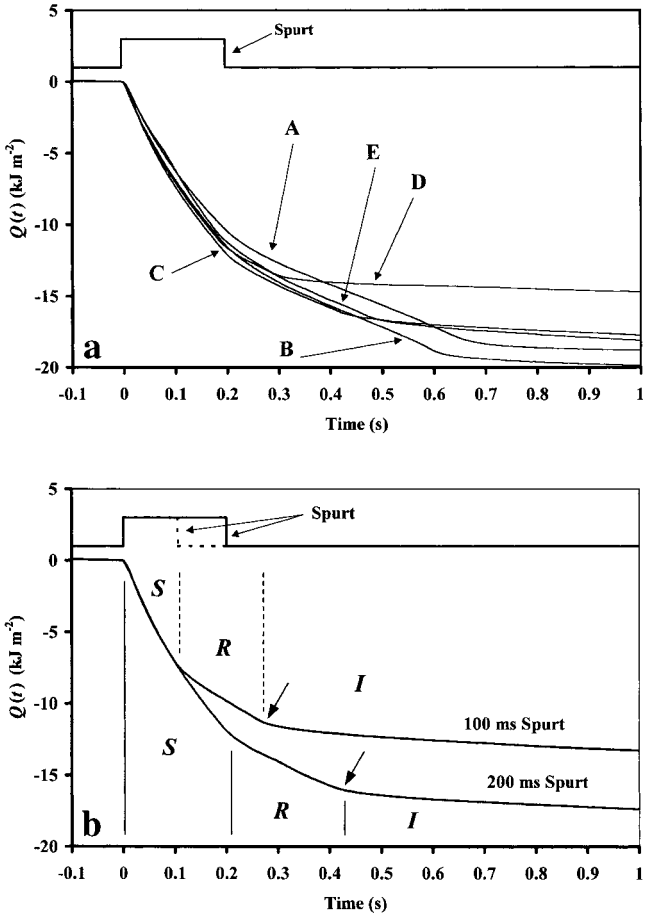

Fig. 7. Heat removal as a function of time ($Q(t)$) at spraying distance $D_{Q_{\max}}$ for: (a) cryogen delivery devices A–E in response to a 200-ms spurt; and (b) device C in response to 100 and 200-ms spurts; In (b) intervals S, R, and I correspond to spraying time, cryogen residence time, and duration of ice on the substrate surface, respectively. Arrows indicate the time when ice formation began.

much as skin types with higher melanin concentrations absorb greater amounts of energy in the epidermis, the chance of non-specific injury is increased. Studies have shown that with current clinical light doses, non-specific injury is a concern during laser treatment of patients with Fitzpatrick skin types IV–VI [33,34]. Increasing the amount of heat removed from the epidermal basal junction would allow darker skin types to benefit from cutaneous laser therapy.

Solely considering an increased ΔT_{0^-}, achieved by increasing the spraying distance, a greater Q would be expected; however, this was not the case. Therefore, other parameters may also affect Q. Although Q decreases past its peak value ($Q_{\max}$), ΔT_{0^-} may reach a plateau or even continue to increase as a function of spraying distance (Fig. 5). An explanation for this discrepancy may be as follows. If large droplets and/or those with high velocity (e.g., coming through shorter spraying distance) impinge on the accumulated film, they may have sufficient kinetic energy to penetrate deeply into the film, and come in closer physical contact with the substrate surface, resulting in more efficient thermal transfer from the cold droplets into the substrate [17]. If droplets with a low kinetic energy (e.g., coming through longer spraying distance) impinge on the accumulated film, the cold droplets will not be able to penetrate as deeply into the film [17], resulting in less effective thermal transfer to the substrate.

Without considering the input of energy from a laser pulse after the cryogen spurt, a greater cryogen mass output will remove more heat at the end of the cryogen residence time (R interval) as shown in Figure 7. A greater mass on the surface may also help protect the epidermis *after* irradiation by creating a heat sink. Demonstrated in Figure 7b is a higher rate of heat removal during the spurt (S interval) than the residence time (R interval). Prolonging the time of most efficient cooling (S interval), and increasing the cryogen mass on the surface (i.e., from a longer spurt) will increase protection to the epidermis from thermal injury by lowering the epidermal basal layer temperature, and creating a heat sink on the surface of the skin. This is confirmed in an ex vivo study [12] in which a 100-ms spurt combined with a 150-ms delay until onset of the laser pulse was compared to a 250-ms spurt with no delay. The 250-ms spurt was able to markedly increase the protection to the epidermis (characterized by minimal basal keratinocyte vacuolization, and no separation of epidermis from dermis) in response to laser irradiation at high fluences, compared to the 100 ms spurt plus 150 ms delay. Our study has shown that for cryogen R-134a, when T_{film} is limited to a value above $-55°C$, increased epidermal cooling is achieved by using longer spurts [12,31].

Although there appears a to be a pattern relating Q to droplet diameter and spray density (Fig. 4), combined effects of multiple parameters such as droplet size, droplet velocity, kinetic energy, surface tension, spray density, and volumetric flux of cryogen may be required to maximize heat removal by a cryogen delivery device. Our next set of studies will focus on velocity measurements with

emphasis on multiple parameters to be correlated with heat removal.

CONCLUSION

This study has shown that heat removal varies among various cryogen delivery devices. This variation in heat removal, however, is modest (14%) despite the relatively large differences in mass output (greater than a factor of 6) and droplet sizes (greater than a factor of 2) among the devices. A non-linear relationship between heat removal by various devices and droplet size and spray density was observed. This study also demonstrated that the heat removal during the spraying period (*S* interval) is much larger than that during cryogen residence time on the substrate surface (*R* interval).

REFERENCES

1. Lask G, Elman M, Slatkine M, Waldman A, Rozenberg Z. Laser-assisted hair removal by selective photothermolysis. Dermatol Surg1997;23:737–739.
2. Valeria BC, Dierickx CC, Farinelli WA, Tai-Yuan DL, Woraphong M, Anderson RR. Ruby laser hair removal: evaluation of long-term efficacy and side effects. Lasers Surg Med 2000;26:177–185.
3. Ross EV, Sajben FP, Hsia J, Barnette D, Hiller CH, McKinlay JR. Nonablative skin remodeling: selective dermal heating with a mid-infrared laser and contact cooling combination. Lasers Surg Med 2000;26:186–195.
4. Stafford TJ, Lizek R, Boll J, and Tan OT. Removal of colored tattoos with the Q-switched alexandrite laser. Plast Reconstr Surg1995;95:313–320.
5. Dover JS, Arndt KA. New approaches to the treatment of vascular lesions. Lasers Surg Med 2000;26:158–163.
6. Anderson RR, Parrish JA. Selective photothermolysis: precise microsurgery by selective absorption of pulsed radiation. Science. 1983;220:524–527.
7. Niemz MH. Laser-Tissue Interactions. Berlin: Springer-Verlag. 1996.
8. Zenzie HH, Altshuler GB, Smirnov MZ, Anderson RR. Evaluation of cooling methods for laser dermatology. Lasers Surg Med 2000;26:130–144.
9. Altshuler GB, Zenzie HH, Erofeev AV, Smirnov MZ, Anderson RR, Dierickx C. Contact cooling of the skin. Phys Med Biol 1999;44:1003–1023.
10. Nelson JS, Milner TE, Anvari B, Tanenbaum BS, Svaasand LO, Kimel S. Dynamic epidermal cooling in conjunction with laser-induced photothermolysis of port wine stain blood vessels. Lasers Surg Med 1996;19:224–229.
11. Anvari B, Tanenbaum BS, Milner TE, Tang K, Liaw LH, Kalafus K, Kimel S, Nelson JS. Spatially selective photocoagulation of biological tissues: feasibility study utilizing cryogen spray cooling. Appl Opt 1996;35:3314–3320.
12. Tunnell JW, Nelson JS, Torres JH, Anvari B. Epidermal protection with cryogen spray cooling during high fluence pulsed dye laser irradiation: an ex vivo study. Lasers Surg Med 2000;27:373–383.
13. Chang CJ, Anvari B, Nelson JS. Cryogen spray cooling for spatially selective photocoagulation of hemangiomas: a new methodology with preliminary clinical reports. Plast Reconstr Surg 1998;102:459–463
14. Kelly KM, Nelson JS, Lask GP, Geronemus RG, Bernstein LJ. Cryogen spray cooling in combination with nonablative laser treatment of facial rhytides. Arch Dermatol 1999;135:691–694.
15. Torres JH, Anvari B, Tanenbaum BS, Milner TE, Yu JC, Nelson JS. Internal temperature measurements in response to cryogen spray cooling of a skin phantom. SPIE Proc 1999;3590:11–19.
16. Anvari B, Milner TE, Tanenbaum BS, Nelson JS. A comparative study of human skin thermal response to sapphire contact and cryogen spray cooling. IEEE Trans Biomed Eng 1998;45:934–941.
17. Verkruysse W, Majaron B, Aguilar G, Svaasand LO, Nelson JS. Dynamics of cryogen deposition relative to heat extraction rate during cryogen spray cooling. SPIE Proc 2000;3907:37–48.
18. Torres JH, Nelson JS, Tanenbaum BS, Milner TE, Goodman DM, Anvari B. Estimation of internal skin temperatures in response to cryogen spray cooling: implications for laser therapy of port wine stains. IEEE J Spec Topics Quant Elect 1999;5:1058–1066.
19. Nelson JS, Kimel S. Safety of cryogen spray cooling during pulsed laser treatment of selected dermatoses. Lasers Surg Med 2000;26:2–3.
20. Alexander DJ, Libretto SE. An overview of the toxicology of HFA-134a (1,1,1,2-tetrafluoroethane). Hum Exp Toxicol 1995;14:715–720.
21. Lefebvre AH. Atomization and Sprays. New York: Hemisphere Publishing Corporation. 1989.
22. Estes KA and Mudawar I. Correlation of Sauter mean diameter and critical heat flux for spray cooling of small surfaces. Int J Heat Mass Transf 1995;38:2985–2996.
23. Duck FA. Physical Properties of Tissue. A Comprehensive Reference Book. London: Academic Press. 1990.
24. Taler J. Theory of transient experimental techniques for surface heat transfer. Int J Heat Mass Transf 1996;39:3733–3748.
25. Beck JV, Blackwell B, St. Clair CR Jr. Inverse Heat Conduction: Ill-Posed Problems. New York: Wiley, Inc. 1985.
26. Mehrotra SP, Chakravarty A, Singh P. Determination of the interfacial heat transfer coefficient in a metal-metal sytem solving the inverse heat conduction problem. Steel Res 1997;68:201–208.
27. Osman AM, Beck JV. Investigation of transient heat transfer coefficients in quenching experiments. Trans ASME J Heat Transf 1990;112:843–848.
28. Hernandez-Morales B, Brimacombe JK, Hawbolt EB. Characterization of the boundary condition in heat treatment operations using an inverse heat conduction algorithm. Proc. ASME Heat Transf Div 1995;317:559–563.
29. Tunnell JW, Torres JH, Anvari B. Inverse heat transfer formulation for measurement of boundary heat flux during cryogen spray cooling. Ann Biomed Eng (in review).
30. Ozisik MN. Heat Conduction. New York: Wiley, 2nd Ed. 1993.
31. Verkruysse W, Majaron B, Tanenbaum BS, Nelson JS. Optimal cryogen spray cooling parameters for pulsed laser treatment of port wine stains. Lasers Surg Med 2000;27:165–170.
32. Torres JH, Tunnell JW, Pikkula BM, Anvari B. An analysis of heat removal during cryogen spray cooling and effects of simultaneous airflow application (in press).
33. Chung JH, Koh WS, Youn JI. Histological responses of port wine stains in brown skin after 578 nm copper vapor laser treatment. Lasers Surg Med 1996;18:358–366.
34. Ashinoff, R. and R.G. Geronemus. Treatment of a port-wine stain in a black patient with the pulsed dye laser. J Dermatol Surg Oncol 1992;18:147–148.